

An Expanded 2D Fused Aromatic Network with 90-Ring Hexagons

Alberto Riaño, Karol Strutyński, Meng Liu, Craig T. Stoppiello, Belén Lerma-Berlanga, Akinori Saeki, Carlos Martí-Gastaldo, Andrei N. Khlobystov, Giovanni Valenti, Francesco Paolucci, Manuel Melle-Franco, and Aurelio Mateo-Alonso*

Abstract: Two-dimensional fused aromatic networks (2D FANs) have emerged as a highly versatile alternative to holey graphene. The synthesis of 2D FANs with increasingly larger lattice dimensions will enable new application perspectives. However, the synthesis of larger analogues is mostly limited by lack of appropriate monomers and methods. Herein, we describe the synthesis, characterisation and properties of an expanded 2D FAN with 90-ring hexagons, which exceed the largest 2D FAN lattices reported to date.

Introduction

Two-dimensional fused aromatic networks (2D FANs)^[1] are a class of conjugated 2D polymers that have emerged as a highly versatile alternative to holey graphene. Similarly, 2D FANs combine an extended 2D π -system with permanent nanometer-sized pores, and have shown charge carrier mobility values reaching $1000 \text{ cm}^2 \text{ V}^{-1} \text{ s}^{-1}$.^[2] 2D FANs are synthesised from organic monomers that act as nodes and linkers and that can be designed at will. Hence by controlling the monomer structure and geometry, 2D FANs with different but predictable lattices and pore sizes can be obtained. In addition, heteroatoms, and substituents can be incorporated into the framework by modification of the monomers, which provides an additional way to modulate their electronic structure and their properties.

Among these, pyrazine-fused 2D FANs^[1a,e] (Figure 1) are receiving increasing attention as they can be obtained by imine-type cyclocondensation reactions between monomers

equipped with sets of *o*-quinone and *o*-diamine groups.^[3] On one hand this type of condensation fuses together the π -systems of both monomers through the formation of a pyrazine ring. On the other hand, the pyrazine linkage introduces simultaneously two electron-withdrawing nitrogen atoms in the framework. This exchange of C atoms for N atoms in specific sites has given rise to materials with a lot of potential in electronics,^[2,4] photovoltaics,^[5] gas separation and storage,^[6] membranes for proton conduction^[7] and water purification,^[8] organic catalysts,^[9] and metal-free electrodes for the oxygen reduction reaction,^[10] oxygen evolution reaction,^[11] supercapacitors,^[12] and batteries.^[13]

Increasing the pore size of 2D FANs would allow the diffusion and encapsulation of organic, inorganic and biological macromolecules and would make available materials that combine both larger band gaps^[14] and porosities, broadening the application scope of 2D FANs into other fields, such as sensing and heterogeneous catalysis. However, synthesising 2D FANs with larger dimensions is a difficult task. Firstly, because of the limited number of monomers, the poor solubility of increasingly large monomers, and the harsh polymerisation conditions that are not always compatible with the functional groups of increasingly complex monomers. And secondly, in analogy to other framework materials, large pore 2D FANs are more prone to collapse upon activation. Nevertheless, an impressive wealth of honeycomb 2D FANs with hexagons constituted of 12-,^[4a] 18-,^[7,11,13a] 24-,^[4b,7,10,12,13b-d,15] 30-,^[2] 36-,^[9,12b] 42-,^[5] and 54-fused^[8] rings (highlighted in yellow in Figure 1) have been reported to date.

[*] Dr. A. Riaño, Prof. Dr. A. Mateo-Alonso
 POLYMAT, University of the Basque Country UPV/EHU
 Avenida de Tolosa 72, 20018 Donostia-San Sebastián (Spain)
 E-mail: amateo@polymat.eu

Dr. K. Strutyński, Prof. Dr. M. Melle-Franco
 CICECO-Aveiro Institute of Materials
 Department of Chemistry, University of Aveiro
 3810-193 Aveiro (Portugal)

M. Liu, Dr. G. Valenti, Prof. Dr. F. Paolucci
 Dipartimento di Chimica "Giacomo Ciamician"
 Via Selmi 2, 40126 Bologna (Italy)



Dr. C. T. Stoppiello, Prof. Dr. A. N. Khlobystov
 School of Chemistry, University of Nottingham
 University Park, Nottingham (UK)


Dr. C. T. Stoppiello
 Nanoscale and Microscale Research Centre
 University of Nottingham
 University Park, Nottingham (UK)

B. Lerma-Berlanga, Dr. C. Martí-Gastaldo
 Instituto de Ciencia Molecular (ICMol)
 Universitat de València
 Paterna 46980, València (Spain)

Prof. Dr. A. Saeki
 Department of Applied Chemistry
 Graduate School of Engineering, Osaka University
 Suita, Osaka 565-0871 (Japan)

Prof. Dr. A. Mateo-Alonso
 Ikerbasque, Basque Foundation for Science
 48009 Bilbao (Spain)

 Supporting information and the ORCID identification number(s) for the author(s) of this article can be found under:
 <https://doi.org/10.1002/anie.202113657>

 © 2021 The Authors. Angewandte Chemie International Edition published by Wiley-VCH GmbH. This is an open access article under the terms of the Creative Commons Attribution Non-Commercial License, which permits use, distribution and reproduction in any medium, provided the original work is properly cited and is not used for commercial purposes.

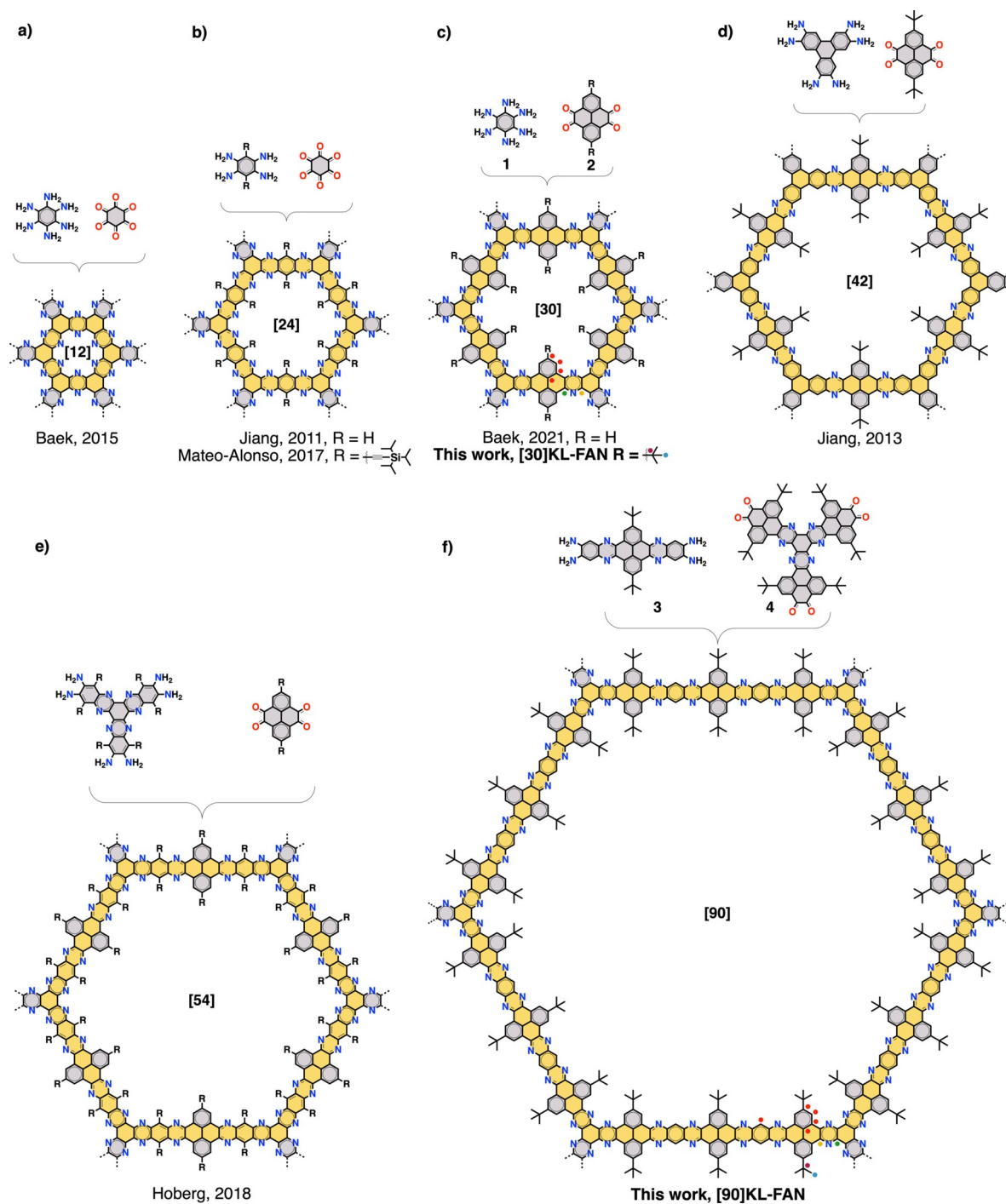


Figure 1. Representative examples of 2D FANs with hexagons constituted of a) 12-,^[4a] b) 24-,^[10a,12a] c) 30-,^[2] d) 42-,^[5] and e) 54-fused^[8] rings and the structures of c) [30]KL-FAN and f) [90]KL-FAN described in this work. The coloured dots in (c) and (f) indicate the assignments of the signals on Figures 2 c and 3 c.

Herein we report the synthesis of a 2D FAN with 90-ring hexagons (Figure 1 f, [90]KL-FAN, where KL stands for Koke Lab), the largest yet reported. [90]KL-FAN has been obtained by solvothermal cyclocondensation of a new set of large synthetic monomers that show an optimal solubility in the reaction media. The structural, optoelectronic and redox features of [90]KL-FAN have been compared with those of

a reference 2D FAN with 30-ring sides (Figure 1, [30]KL-FAN). The comparison reveals a lower band gap, a higher nitrogen uptake, and improved electrochemical properties for [90]KL-FAN, while maintaining a similar degree of crystallinity and similar charge transporting properties, despite the larger dimensions.

Results and Discussion

[30]KL-FAN was obtained by solvothermal condensation of hexaaminobenzene **1**^[16] and pyrene tetraone **2**^[17] (Figure 1c) in *N*-methyl-2-pyrrolidone (NMP) with a catalytic amount of H₂SO₄ at 250 °C. In this particular case, the reaction mixture must be kept at 0 °C before heating in order to ensure the reproducibility of the reaction. We attributed this behaviour to the high reactivity of hexaaminobenzene **1**. [90]KL-FAN was synthesised by condensation between dibenzotetraazahexacene tetraamine **3**^[18] and hexabenzohexaazatetraacetylene hexaone **4**^[19] (Figure 1f) in *N*-methyl-2-pyrrolidone (NMP) with a catalytic amount of H₂SO₄ at 170 °C. In this case, the reaction proceeded without the need of precooling the mixture, which is consistent with the lower reactivity of tetraamine **3** in comparison to hexaamine **1**. [30]KL-FAN and [90]KL-FAN were obtained as black powders after Soxhlet extraction. The structures of [30]KL-FAN and [90]KL-FAN were confirmed by a combination of different characterisation techniques.

The FT-IR spectra of [30]KL-FAN and [90]KL-FAN (Figure 2a and Figure 3a) show the attenuation of the N–H (around 3100 cm⁻¹) and C=O (around 1700 cm⁻¹) bands of the corresponding monomers, which indicate that an efficient polymerisation has taken place.

Solid-state cross-polarisation/magic-angle spinning (SS CP/MAS) NMR spectroscopy of [30]KL-FAN and [90]KL-FAN is consistent with the proposed structure. The SS CP/MAS ¹H NMR spectra show two signals that correspond to the aromatic and *tert*-butyl protons of the FANs in

both cases because of the structural similarities (Figures 2b and 3b). The SS CP/MAS ¹³C NMR spectra also show a similar set of signals for both 2D FANs in agreement with their structural similarities, namely three signals in the 150–120 ppm region that correspond to the aromatic carbons and two signals around 30 ppm that correspond to the *tert*-butyl carbons (Figures 2c and 3c). The absence of a sharp signal around 190 ppm indicates a low number of carbonyl groups in both FANs, which also indicates a good conversion.

X-ray photoelectron spectroscopy (XPS; Figures S1 and S2) and energy-dispersive X-ray spectroscopy (EDX; Figure S3) confirm the presence of carbon, nitrogen and oxygen. The occurrence of carbon and nitrogen is consistent with the chemical composition of [30]KL-FAN and [90]KL-FAN. The presence of oxygen has been attributed to existence of unreacted ketone and amino groups and to the entrapment of water molecules, as illustrated by the deconvolution of the nitrogen and oxygen peaks (Figures S1 and S2). Elemental analysis showed that the carbon and nitrogen ratios were consistent with theoretical values, although the absolute percentages of carbon were lower than theoretical values (Tables S1 and S2). This discrepancy between the theoretical and observed values is also consistent with the presence of unreacted ketone and amino groups and of water, as indicated by XPS (Figures S1 and S2), thermal gravimetric analysis (Figure S4) and previous observations.^[4a,d]

In order to assess the porosity of [30]KL-FAN and [90]KL-FAN, N₂ gas adsorption measurements at 77 K were performed. The isotherms confirm that [30]KL-FAN and [90]KL-FAN are porous materials (Figures 2d and 3d) that

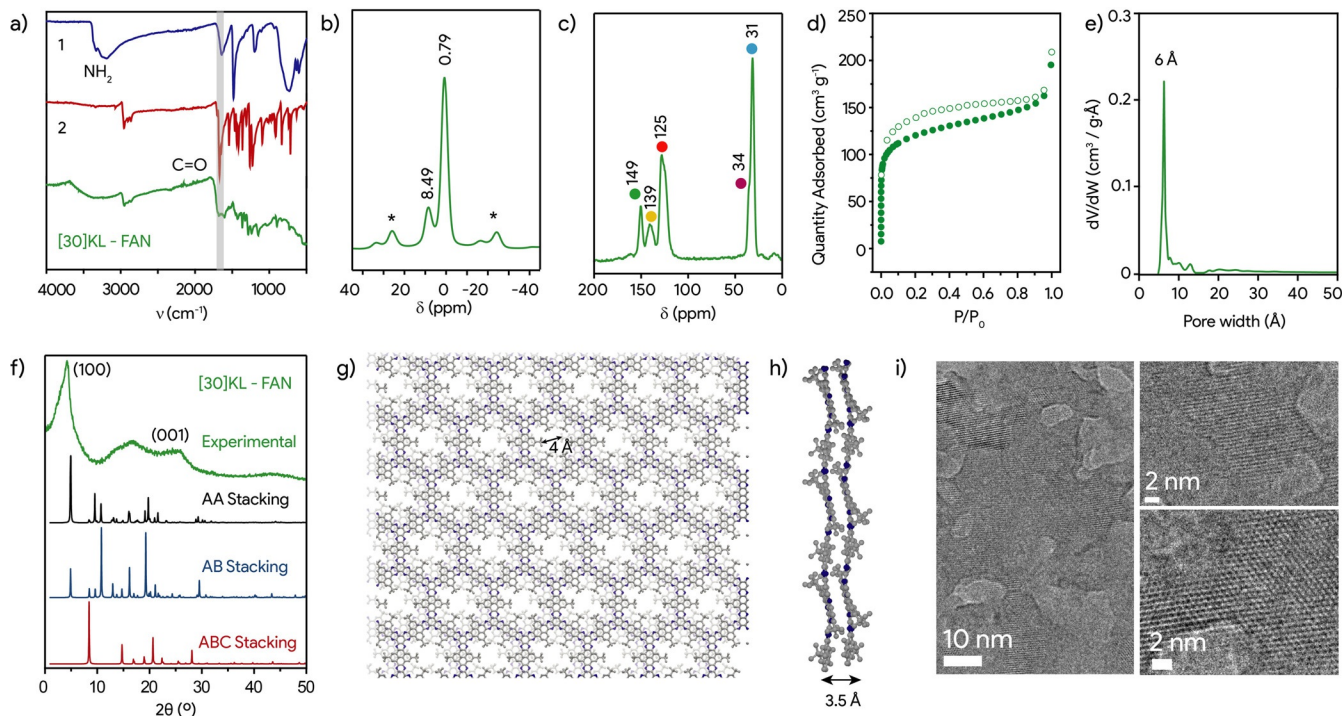


Figure 2. Experimental and simulated structural characterisation of [30]KL-FAN. a) FTIR; b) SS CP/MAS ¹H NMR (* denotes side peaks); c) SS CP/MAS ¹³C NMR (the coloured dots on each signal correspond to the carbons marked in Figure 1c); d) nitrogen adsorption and desorption isotherm profiles at 77 K; e) pore size distribution; f) experimental and simulated PXRD patterns; theoretical models showing the g) face-on and h) side-on projections; i) HRTEM images.

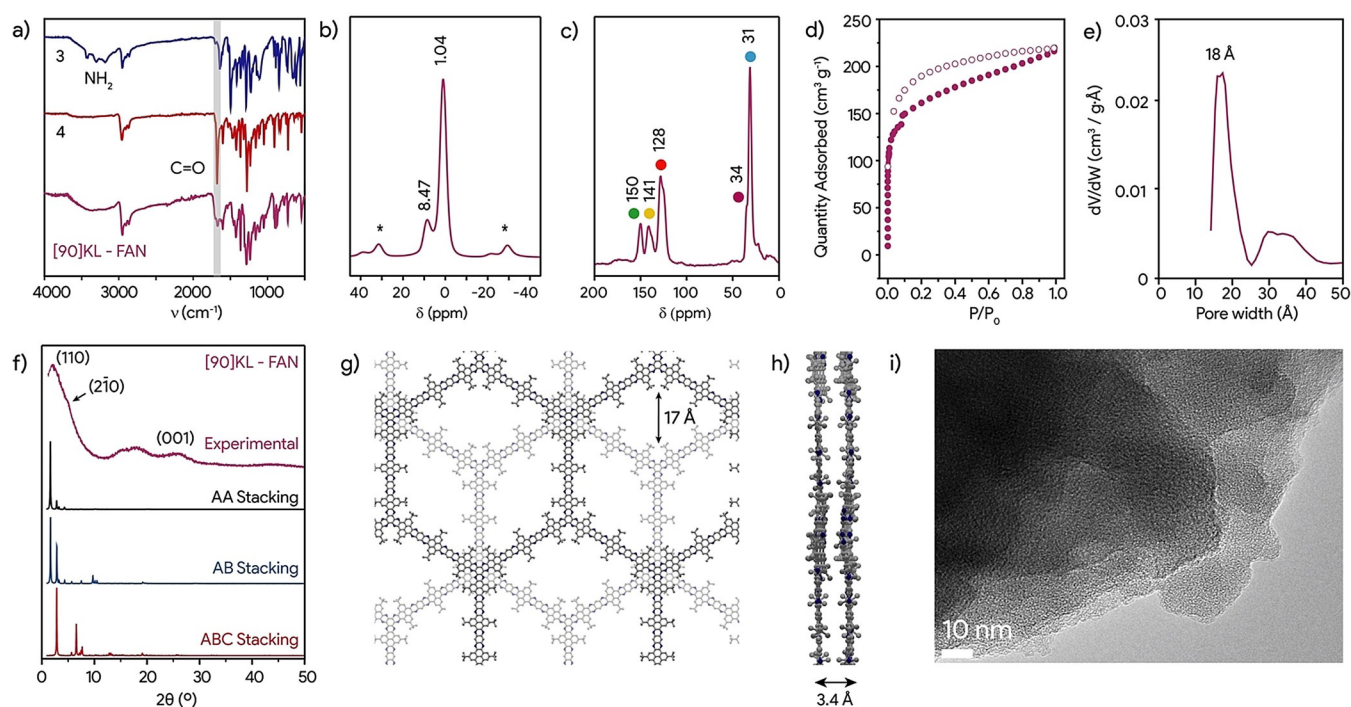


Figure 3. Experimental and simulated structural characterisation of [90]KL-FAN. a) FTIR; b) SS CP/MAS ^1H NMR (* denotes side peaks); c) SS CP/MAS ^{13}C NMR (the coloured dots on each signal correspond to the carbons marked in Figure 1 f); d) nitrogen adsorption and desorption isotherm profiles at 77 K; e) pore size distribution; f) experimental and simulated PXRD patterns; theoretical models showing the g) face-on and h) side-on projections; i) HRTEM image.

show, respectively, Brunauer–Emmet–Teller (BET) surface areas of 449 and $567\text{ m}^2\text{ g}^{-1}$ and NLDFT pore sizes centred at 6 and 18 Å (Figures 2 e and 3 e).

The powder X-ray diffraction (PXRD) of [30]KL-FAN and [90]KL-FAN reveals patterns of broad peaks that are similar to those observed in other 2D FANs.^[2,4b-d,e,5,7,8,12b,13d,15b] The XRD peaks of 2D FANs are usually broad as the result of the limited reversibility of the pyrazine linkers and turbostratic disorder. In both cases, the diffractograms show two main diagnostic peaks that support the formation of the microporous honeycomb network. The first one, the low-angle peak at 6.08° in the case of [30]KL-FAN and at 1.77° in the case of [90]KL-FAN, corresponds in both cases to the (100) reflection (Figures 2 f and 3 f). The second one, the peak around 25° , corresponds to the (001) reflection and to the *d*-spacing of π -stacked aromatic systems ($\approx 3.4\text{ \AA}$).

To shine additional light on the structure of [30]KL-FAN and [90]KL-FAN, three general packing configurations (AA, AB and ABC) were computationally explored and their simulated PXRD patterns were compared with the experimental ones. In the case of [30]KL-FAN, the simulated diffractogram for the slipped AA packing mode shows a better fit with the experimental one. Meanwhile, in the case of [90]KL-FAN, the experimental diffractogram shows a better fit with the simulated diffractogram for the AB packing mode. This assignment is consistent with the NLDFT pore size distributions estimated from nitrogen adsorption measurements. In fact, the pore size of the [30]KL-FAN model in an AA configuration (4 \AA) is in excellent agreement with the experimental pore size (6 \AA ; Figure 2 e,g). Also, the

pore size of the [90]KL-FAN model in an AB configuration (17 \AA) is in excellent agreement with the experimental pore size (18 \AA ; Figure 3 e,g).

High-resolution transmission electron microscopy (HRTEM) images of [30]KL-FAN and [90]KL-FAN evidence their 2D layered structure by the presence of terraces and step-edges of overlapping sheets (Figures 2 i and 3 i). In both cases, the micrographs show the projections of irregular pores, which were turbostratically disordered. In some particular areas of [30]KL-FAN, seemingly crystalline regions can be observed (Figure 2 i) with some periodic features being attributed to the stacking arrangements of the individual layers. The unexpected mesopores within the structure (Figure 2 i) are likely to be caused by the presence of solvent molecules during the formation of the FAN lattice and terminated by unreacted carbonyl groups due to incomplete condensation, as we previously demonstrated for a conjugated microporous polymer.^[20]

The optical properties of [30]KL-FAN and [90]KL-FAN were studied by UV/Vis-NIR spectroscopy (Figure 4 a,b). Thin films were obtained by drop-casting dispersions of [30]KL-FAN and [90]KL-FAN in trifluoroacetic acid (TFA) directly onto a glass slide, which allowed estimating the optical band gap using Tauc's method (inset Figure 4 a,b). Band gaps of 2.05 and 1.95 eV were estimated, respectively, for [30]KL-FAN and [90]KL-FAN that illustrate their semi-conducting nature.

The electrochemical properties of [30]KL-FAN and [90]KL-FAN were investigated by cyclic voltammetry in a rotating ring-disk electrode (RRDE; Figure 4 c and Ta-

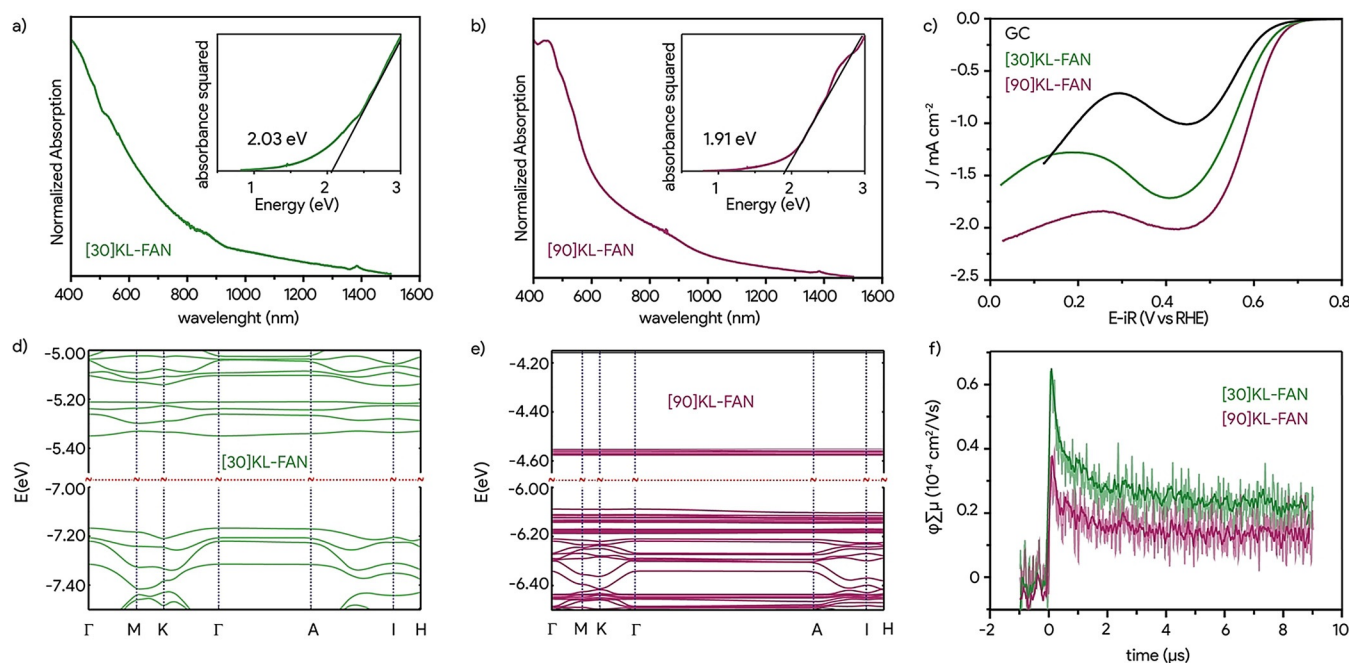


Figure 4. UV/Vis-NIR electronic absorption spectra of a) [30]KL-FAN and b) [90]KL-FAN. Inset corresponds to Tauc's plot. c) RRDE voltammograms (disk currents) recorded in O_2 -saturated 0.1 M KOH at 1600 rpm. The disk potential was scanned at 10 mVs^{-1} and the ring potential was constant at 1.4 V versus RHE. Band structures of d) [30]KL-FAN and e) [90]KL-FAN. f) TMRC measurements ($\lambda = 355 \text{ nm}$, $I_0 = 9.1 \times 10^{15} \text{ photons cm}^{-2}$).

ble S3). For this purpose, freshly prepared dispersions of [30]KL-FAN and [90]KL-FAN in TFA were directly drop-casted on a glassy carbon (GC) RRDE. The voltametric curves in an argon-saturated aqueous 0.1 M KOH solution show no redox processes. However, in an oxygen-saturated solution, the voltammograms reveal a reduction wave characteristic of the oxygen reduction reaction (ORR),^[16,21] which is a key reaction in fuel cells. The voltammograms illustrate that the electrodes containing the 2D FANs show higher potentials at same current densities than the pristine GC electrode. This is consistent with a more efficient ORR as expected for the presence of catalytically active N atoms.^[22] When it comes to the 2D FANs, the electrodes containing [90]KL-FAN show a significantly higher current density at same potential than [30]KL-FAN, for example, at a potential of 0.1 V vs. RHE, their current densities are 2.02 mA cm^{-2} and 1.35 mA cm^{-2} , respectively. The RRDE allows to monitor the formation of H_2O_2 , and hence, to determine the average number of electrons (n) transferred per oxygen molecule with great accuracy. In the case of [90]KL-FAN, $n = 3.00$ (Figure S5). Meanwhile in the case of [30]KL-FAN and GC, $n = 2.75$ and 2.50 , respectively. An electron number n larger than 2 indicates that in all cases the ORR may proceed simultaneously through the 2-electron (from O_2 to H_2O_2) and the 4-electron mechanisms (from O_2 to H_2O) and, the higher the value of n is, the deeper oxygen gets reduced. This means [90]KL-FAN is more efficient than [30]KL-FAN for the ORR. The ORR performance of [90]KL-FAN and [30]KL-FAN is in line with that observed in current state-of-the-art 2D FANs^[10] and other metal-free state-of-the-art 2D materials^[23] with the present additional advantage that no additive or carbonisation treatment was needed. Given the structural

similarities and the similar nitrogen content, the higher electrocatalytic performance of [90]KL-FAN over [30]KL-FAN can be attributed to the larger pore size and surface area that facilitate in the case of [90]KL-FAN the diffusion of oxygen within the framework.

The electronic band structures and the projected density of states of [30]KL-FAN and [90]KL-FAN were calculated by DFT to get an insight into their electronic structure and their charge transporting properties (Figures 4d,e and S6). The calculations illustrate that both [30]KL-FAN and [90]KL-FAN are direct gap semiconductors and show the same trend as the optical band gaps. [30]KL-FAN computed band gap is 1.82 eV at the Γ -point (Figure 4d). The frontier bands show weak dispersions of 37 meV and 15 meV for the highest occupied crystalline orbital (HOCO) and lowest unoccupied crystalline orbital (LUCO) respectively. In contrast, [90]KL-FAN has a lower gap 1.51 eV, also at the Γ -point, and shows degenerate HOCO and LUCO bands (Figure 4e). For the larger FAN, the HOCO band shows further reduced dispersion, 15 meV, while the LUCO band is virtually flat with negligible energy dispersion ($< 1 \text{ meV}$).

The charge transport properties [30]KL-FAN and [90]KL-FAN were probed by flash-photolysis time-resolved microwave conductivity (FP-TRMC).^[24] FP-TRMC allows estimating the pseudo-photoconductivity or intrinsic mobility ($\varphi\Sigma\mu$, where φ : the charge carrier generation yield, $\Sigma\mu$: the sum of charge carrier mobilities). The samples of [30]KL-FAN and [90]KL-FAN showed similar $\varphi\Sigma\mu$ maximum values ($\varphi\Sigma\mu_{\text{max}}$) of 0.6×10^{-4} and $0.4 \times 10^{-4} \text{ cm}^2 \text{ V}^{-1} \text{ s}^{-1}$, respectively (Figure 4f). These $\varphi\Sigma\mu_{\text{max}}$ values are of the same order of magnitude as those observed in molecular nanoribbons and nanographenes with the same fused-ring structure^[19,25] and in

imine 2D covalent organic frameworks.^[26] The similar $\varphi\Sigma\mu_{\max}$ values of [30]KL-FAN and [90]KL-FAN are consistent with their structural similarities in terms of fused-ring structure and interlayer distance.

Conclusion

We have described the successful solvothermal synthesis of a 2D FAN with a honeycomb lattice constituted of 90-ring hexagons, which exceed the largest 2D FAN lattices reported to date. The synthesis of [90]KL-FAN has been achieved by introducing a new set of monomers, which despite their large dimensions are sufficiently soluble in the reaction media. The structure of [90]KL-FAN has been confirmed by a combination of FT-IR, solid-state NMR, porosimetry, PXRD, HRTEM and theoretical studies. [90]KL-FAN-containing electrodes showed enhanced electrocatalytic activity that was attributed to the larger pore size. UV/Vis-NIR electronic absorption, theoretical studies and FP-TRMC show that [90]KL-FAN is a direct band gap semiconductor with an intrinsic charge carrier mobility comparable to those observed in state-of-the-art nanographenes and imine 2D covalent organic frameworks. Overall, this work paves the way for the synthesis of 2D and 3D FANs with increasingly larger lattices. Such large-pore semiconducting FANs may find applications in sensing, electrocatalysis, and energy conversion and storage.

Acknowledgements

This work was carried out with support from the Basque Science Foundation for Science (Ikerbasque), POLYMAT, the University of the Basque Country, Gobierno Vasco (BERC programme) and Gobierno de España (Ministerio de Economía y Competitividad CTQ2016-77970-R). This work was performed under the Maria de Maeztu Units of Excellence Programme – Grant No. CEX-2019-000919-M Ministry of Science, Innovation and Universities. Technical and human support provided by SGIker of UPV/EHU and European funding (ERDF and ESF) is acknowledged. This project has received funding from the European Research Council (ERC) under the European Union's Horizon 2020 research and innovation programme (Grant Agreements No. 722951 and No. 714122). This project has received funding from the European Union's Horizon 2020 research and innovation programme under grant agreements No. 664878 and No. 899895. In addition, support through the project IF/00894/2015, the advanced computing project CPCA/A2/2524/2020 granting access to the Navigator cluster at LCA-UC and within the scope of the project CICECO-Aveiro Institute of Materials, UIDB/50011/2020 & UIDP/50011/2020 funded by national funds through the Portuguese Foundation for Science and Technology I.P./MCTES is gratefully acknowledged. The Nanoscale & Microscale Research Centre (nmRC), University of Nottingham, is acknowledged for enabling access to electron microscopy facilities.

Conflict of Interest

The authors declare no conflict of interest.

Keywords: 2D polymers · conjugated 2D polymers · conjugated microporous polymers · fused aromatic networks · polycyclic aromatic hydrocarbons

- [1] a) I. Ahmad, J. Mahmood, J.-B. Baek, *Small Sci.* **2021**, *1*, 2000007; b) L. Cusin, H. Peng, A. Ciesielski, P. Samori, *Angew. Chem. Int. Ed.* **2021**, *60*, 14236–14250; *Angew. Chem.* **2021**, *133*, 14356–14370; c) S. Che, L. Fang, *Chem* **2020**, *6*, 2558–2590; d) M. Martínez-Abadía, A. Mateo-Alonso, *Adv. Mater.* **2020**, *32*, 2002366; e) J. Mahmood, M. A. R. Anjum, J.-B. Baek, *Adv. Mater.* **2018**, *30*, 1805062.
- [2] J. Mahmood, E. K. Lee, H.-J. Noh, I. Ahmad, J.-M. Seo, Y.-K. Im, J.-P. Jeon, S.-J. Kim, J. H. Oh, J.-B. Baek, *Adv. Mater.* **2021**, *33*, 2004707.
- [3] A. Mateo-Alonso, *Chem. Soc. Rev.* **2014**, *43*, 6311–6324.
- [4] a) J. Mahmood, E. K. Lee, M. Jung, D. Shin, I.-Y. Jeon, S.-M. Jung, H.-J. Choi, J.-M. Seo, S.-Y. Bae, S.-D. Sohn, N. Park, J. H. Oh, H.-J. Shin, J.-B. Baek, *Nat. Commun.* **2015**, *6*, 6486; b) S. Jhulki, J. Kim, I.-C. Hwang, G. Haider, J. Park, J. Y. Park, Y. Lee, W. Hwang, A. A. Dar, B. Dhara, S. H. Lee, J. Kim, J. Y. Koo, M. H. Jo, C.-C. Hwang, Y. H. Jung, Y. Park, M. Kataria, Y.-F. Chen, S.-H. Jhi, M.-H. Baik, K. Baek, K. Kim, *Chem* **2020**, *6*, 2035–2045; c) G. Bian, J. Yin, J. Zhu, *Small* **2021**, *17*, 2006043; d) Z. Meng, R. M. Stolz, K. A. Mirica, *J. Am. Chem. Soc.* **2019**, *141*, 11929–11937; e) M. Wang, M. Ballabio, M. Wang, H.-H. Lin, B. P. Biswal, X. Han, S. Paasch, E. Brunner, P. Liu, M. Chen, M. Bonn, T. Heine, S. Zhou, E. Cánovas, R. Dong, X. Feng, *J. Am. Chem. Soc.* **2019**, *141*, 16810–16816.
- [5] J. Guo, Y. Xu, S. Jin, L. Chen, T. Kaji, Y. Honsho, M. A. Addicoat, J. Kim, A. Saeki, H. Ihee, S. Seki, S. Irle, M. Hiramoto, J. Gao, D. Jiang, *Nat. Commun.* **2013**, *4*, 2736.
- [6] S.-J. Kim, T.-H. Kim, I. Ahmad, H.-J. Noh, S.-M. Jung, Y.-K. Im, J. Mahmood, Y.-S. Bae, J.-B. Baek, *Cell Rep. Phys. Sci.* **2021**, *2*, 100502.
- [7] Z. Meng, A. Aykanat, K. A. Mirica, *Chem. Mater.* **2019**, *31*, 819–825.
- [8] V. A. Kuehl, J. Yin, P. H. H. Duong, B. Mastorovich, B. Newell, K. D. Li-Oakey, B. A. Parkinson, J. O. Hoberg, *J. Am. Chem. Soc.* **2018**, *140*, 18200–18207.
- [9] Y. Ma, X. Liu, X. Guan, H. Li, Y. Yusran, M. Xue, Q. Fang, Y. Yan, S. Qiu, V. Valtchev, *Dalton Trans.* **2019**, *48*, 7352–7357.
- [10] a) A. B. Marco, D. Cortizo-Lacalle, I. Perez-Miqueo, G. Valentí, A. Boni, J. Plas, K. Strutyński, S. D. Feyter, F. Paolucci, M. Montes, A. N. Khlobystov, M. Melle-Franco, A. Mateo-Alonso, *Angew. Chem. Int. Ed.* **2017**, *56*, 6946–6951; *Angew. Chem.* **2017**, *129*, 7050–7055; b) V. Briega-Martos, A. Ferre-Vilaplana, A. de la Peña, J. L. Segura, F. Zamora, J. M. Feliu, E. Herrero, *ACS Catal.* **2017**, *7*, 1015–1024.
- [11] C. Yang, Z.-D. Yang, H. Dong, N. Sun, Y. Lu, F.-M. Zhang, G. Zhang, *ACS Energy Lett.* **2019**, *4*, 2251–2258.
- [12] a) Y. Kou, Y. Xu, Z. Guo, D. Jiang, *Angew. Chem. Int. Ed.* **2011**, *50*, 8753–8757; *Angew. Chem.* **2011**, *123*, 8912–8916; b) S. Kandambeth, J. Jia, H. Wu, V. S. Kale, P. T. Parvatkar, J. Czaban-Jóźwiak, S. Zhou, X. Xu, Z. O. Ameer, E. Abou-Hamad, A.-H. Emwas, O. Shekhah, H. N. Alshareef, M. Eddaoudi, *Adv. Energy Mater.* **2020**, *10*, 2001673.
- [13] a) L. Meng, S. Ren, C. Ma, Y. Yu, Y. Lou, D. Zhang, Z. Shi, *Chem. Commun.* **2019**, *55*, 9491–9494; b) X. Li, H. Wang, H. Chen, Q. Zheng, Q. Zhang, H. Mao, Y. Liu, S. Cai, B. Sun, C. Dun, M. P. Gordon, H. Zheng, J. A. Reimer, J. J. Urban, J. Ciston, T. Tan, E. M. Chan, J. Zhang, Y. Liu, *Chem* **2020**, *6*, 933–

- 944; c) R. Shi, L. Liu, Y. Lu, C. Wang, Y. Li, L. Li, Z. Yan, J. Chen, *Nat. Commun.* **2020**, *11*, 178; d) M. K. Shehab, K. S. Weeraratne, T. Huang, K. U. Lao, H. M. El-Kaderi, *ACS Appl. Mater. Interfaces* **2021**, *13*, 15083–15091.
- [14] K. Strutyński, A. Mateo-Alonso, M. Melle-Franco, *Chem. Eur. J.* **2020**, *26*, 6569–6575.
- [15] a) S. Kim, H. C. Choi, *Commun. Chem.* **2019**, *2*, 60; b) J. Mahmood, I. Ahmad, M. Jung, J.-M. Seo, S.-Y. Yu, H.-J. Noh, Y. H. Kim, H.-J. Shin, J.-B. Baek, *Commun. Chem.* **2020**, *3*, 31.
- [16] D. Z. Rogers, *J. Org. Chem.* **1986**, *51*, 3904–3905.
- [17] J. Hu, D. Zhang, F. W. Harris, *J. Org. Chem.* **2005**, *70*, 707–708.
- [18] B. Gao, M. Wang, Y. Cheng, L. Wang, X. Jing, F. Wang, *J. Am. Chem. Soc.* **2008**, *130*, 8297–8306.
- [19] J. P. Mora-Fuentes, A. Riaño, D. Cortizo-Lacalle, A. Saeki, M. Melle-Franco, A. Mateo-Alonso, *Angew. Chem. Int. Ed.* **2019**, *58*, 552–556; *Angew. Chem.* **2019**, *131*, 562–566.
- [20] C. T. Stoppiello, H. Isla, M. Martínez-Abadía, M. W. Fay, C. D. J. Parmenter, M. J. Roe, B. Lerma-Berlanga, C. Martí-Gastaldo, A. Mateo-Alonso, A. N. Khlobystov, *Nanoscale* **2019**, *11*, 2848–2854.
- [21] a) S. Zhao, D.-W. Wang, R. Amal, L. Dai, *Adv. Mater.* **2019**, *31*, 1801526; b) C. Hu, L. Dai, *Adv. Mater.* **2019**, *31*, 1804672; c) D. Liu, K. Ni, J. Ye, J. Xie, Y. Zhu, L. Song, *Adv. Mater.* **2018**, *30*, 1802104; d) X. Liu, L. Dai, *Nat. Rev. Mater.* **2016**, *1*, 16064; e) L. Dai, Y. Xue, L. Qu, H.-J. Choi, J.-B. Baek, *Chem. Rev.* **2015**, *115*, 4823–4892; f) Y. Zhang, J. Zhang, D. S. Su, *ChemSusChem* **2014**, *7*, 1240–1250; g) P. Ayala, R. Arenal, M. Rummeli, A. Rubio, T. Pichler, *Carbon* **2010**, *48*, 575–586; h) M. Antonietti, M. Oschatz, *Adv. Mater.* **2018**, *30*, 1706836.
- [22] a) Q. Lv, W. Si, J. He, L. Sun, C. Zhang, N. Wang, Z. Yang, X. Li, X. Wang, W. Deng, Y. Long, C. Huang, Y. Li, *Nat. Commun.* **2018**, *9*, 3376; b) J. Quílez-Bermejo, M. Melle-Franco, E. San-Fabián, E. Morallón, D. Cazorla-Amorós, *J. Mater. Chem. A* **2019**, *7*, 24239–24250.
- [23] a) S. M. Lyth, Y. Nabaee, S. Moriya, S. Kuroki, M.-a. Kakimoto, J.-i. Ozaki, S. Miyata, *J. Phys. Chem. C* **2009**, *113*, 20148–20151; b) Y. Zheng, Y. Jiao, J. Chen, J. Liu, J. Liang, A. Du, W. Zhang, Z. Zhu, S. C. Smith, M. Jaroniec, G. Q. Lu, S. Z. Qiao, *J. Am. Chem. Soc.* **2011**, *133*, 20116–20119; c) Z. Xiang, D. Cao, L. Huang, J. Shui, M. Wang, L. Dai, *Adv. Mater.* **2014**, *26*, 3315–3320; d) Z. Xiang, Y. Xue, D. Cao, L. Huang, J.-F. Chen, L. Dai, *Angew. Chem. Int. Ed.* **2014**, *53*, 2433–2437; *Angew. Chem.* **2014**, *126*, 2465–2469; e) S. Yang, X. Feng, X. Wang, K. Müllen, *Angew. Chem. Int. Ed.* **2011**, *50*, 5339–5343; *Angew. Chem.* **2011**, *123*, 5451–5455.
- [24] A. Saeki, Y. Koizumi, T. Aida, S. Seki, *Acc. Chem. Res.* **2012**, *45*, 1193–1202.
- [25] D. Cortizo-Lacalle, J. P. Mora-Fuentes, K. Strutyński, A. Saeki, M. Melle-Franco, A. Mateo-Alonso, *Angew. Chem. Int. Ed.* **2018**, *57*, 703–708; *Angew. Chem.* **2018**, *130*, 711–716.
- [26] a) S. Dalapati, M. Addicoat, S. Jin, T. Sakurai, J. Gao, H. Xu, S. Irle, S. Seki, D. Jiang, *Nat. Commun.* **2015**, *6*, 7786; b) H. Ding, Y. Li, H. Hu, Y. Sun, J. Wang, C. Wang, C. Wang, G. Zhang, B. Wang, W. Xu, D. Zhang, *Chem. Eur. J.* **2014**, *20*, 14614–14618; c) S. Jin, T. Sakurai, T. Kowalczyk, S. Dalapati, F. Xu, H. Wei, X. Chen, J. Gao, S. Seki, S. Irle, D. Jiang, *Chem. Eur. J.* **2014**, *20*, 14608–14613; d) S. Wan, F. Gándara, A. Asano, H. Furukawa, A. Saeki, S. K. Dey, L. Liao, M. W. Ambrogio, Y. Y. Botros, X. Duan, S. Seki, J. F. Stoddart, O. M. Yaghi, *Chem. Mater.* **2011**, *23*, 4094–4097.

Manuscript received: October 8, 2021

Revised manuscript received: October 29, 2021

Accepted manuscript online: November 8, 2021

Version of record online: December 2, 2021